ACS OMEGA

Open Access

http://pubs.acs.org/journal/acsodf

Article

A Novel Biochar from Agro-Industrial Waste: Synthesis, Characterization, and Application for Acetylsalicylic Acid Removal

Published as part of ACS Omega special issue "Chemistry in Brazil: Advancing through Open Science".

Matheus Londero da Costa, Leandro Rodrigues Oviedo, Giovani Pavoski, Jorge Alberto Soares Tenório, Denise Crocce Romano Espinosa, Yolice Patricia Moreno, Daniel Moro Druzian, Sthéfany Nunes Loureiro, and William Leonardo da Silva*

Cite This: *ACS Omega* 2025, 10, 57532−57544

Read Online

ACCESS | Metrics & More | Article Recommendations | Supporting Information

ABSTRACT: Due to drugs not being completely metabolized and excreted in their original form or as byproducts that contaminate water resources, the conventional treatment process often fails to remove these pollutants. Consequently, some studies seek to use waste to create materials capable of purifying water. Adsorption, being a process of low complexity and operational cost, stands out as a widely used process for wastewater treatment. In this context, the present work aims to synthesize and characterize a novel biochar from *Lagenaria siceraria* for the removal of the acetylsalicylic acid (ASA) drug by the adsorption process (kinetic, equilibrium, and thermodynamic) and to evaluate its ecotoxicity in *Artemia salina*. The biochar showed a heterogeneous, porous, and negatively charged surface (−18.76 ± 8.05 mV), with a surface area of 0.35 $m^2\ g^{-1}$ and pH_{ZCP} = 6.95. It achieved 42% ASA removal under ideal conditions (10 mg L^{-1} ASA, 0.25 g L^{-1} biochar, and pH 4) and exhibited a maximum capacity (q_{max}) of 137.33 mg g^{-1}. In the thermodynamic study, there was a greater removal rate of 77% at 35 °C, and the best model was the Khan model in adsorption equilibrium (R^2 = 0.999), which indicates mono- and multilayer adsorption by electrostatic action. At low ASA concentrations, the pseudo-first-order (PFO) model presented the best fit, indicating a predominance of fast adsorption at surface sites and physical interactions. Meanwhile, for higher concentrations of ASA, the pseudo-second-order (PSO) model was more adequate, suggesting an increasing contribution of specific chemical interactions at higher-energy sites. The biosorbent showed no ecotoxicity between 100−1000 mg L^{-1} and a lethal dose of 100% ASA (L_{D100}) at 300 mg L^{-1}. Therefore, biochar can be used as an alternative material for the removal of organic pollutants, such as drug residues.

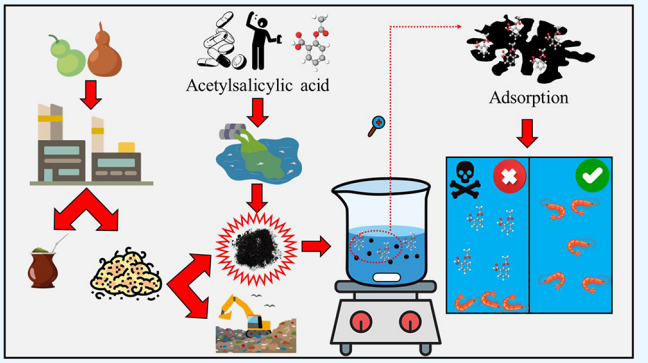

1. INTRODUCTION

Acetylsalicylic acid (ASA) is one of the most consumed drugs around the world (around 50 billion aspirin tablets are consumed each year worldwide),[1] and it is sold in concentrations ranging from 75 to 500 mg L^{-1} around the world.[2,3] As with any drug, ASA is not completely metabolized by the human body, achieving a metabolization rate of 80%, and the remaining amount is excreted unchanged or as byproducts, which in turn reach water bodies, contaminating the environment and affecting people.[4]

Moreover, ecotoxicity tests have been conducted to determine a lethal dose for simpler organisms,[5] such as *Artemia salina* and *Daphnia magna*, which are crustaceans more sensitive to pollution and serve as a food base for other crustaceans and fish.[6,7] Trials with *Daphnia magna* showed a lethal concentration (L_C) of 88.33 mg L^{-1} of ASA after 48 h of exposure.[8]

In this view, there is a need for the development of advanced technologies for wastewater treatment, as conventional water treatment does not entirely remove pollutants due to the low biodegradation rate of 24−48 h.[9,10] Thus, research has been carried out with Advanced Oxidative Processes (AOPs),[11] membranes,[12] and adsorption, which is the most commonly used method due to its low cost and complexity.[13]

In addition, for the adsorption process to occur in a favorable direction, it needs to have certain characteristics, such as being a nanometric material, as it will have a high surface area and a greater presence of pores, which will lead to

Received: August 14, 2025
Revised: November 5, 2025
Accepted: November 13, 2025
Published: November 18, 2025

a greater chance of contact between the adsorbent and the adsorbate, and a higher adsorption capacity.[14] Thus, there are studies that verify the applicability of biochar originating from agro-industrial residues for the removal of drugs such as paracetamol,[15] ibuprofen,[16] sodium diclofenac,[17] and dexamethasone.[18]

Agro-industrial waste is commonly generated during and after the harvesting process, which mainly consists of leaves, roots, bark, and pulp.[19] Worldwide, the region that generates the most agro-industrial waste is found in Asia, with 47%, followed by the American continents with 29%, Europe with 16%, Africa with 6%, and Oceania with 2%.[20,21]

Moreover, agro-industrial waste, such as gourd, can be used as a promising adsorbent for the removal of pharmaceuticals from aqueous solutions, due to its ease of preparation and low cost.[22] Then, the high-temperature carbonization (400−800 °C)[23] commonly done in times of less than 2 h[24] is a process in which a disruption of the original molecular structure of a given material is noticed when carbonaceous materials are subjected to high temperatures to obtain coal or activated carbon.[25] Thus, carbonization is responsible for the opening of the porosity of the raw material, the removal of impurities (low-weight carbonaceous material is converted to CO_2 and water steam), and the improvement of the chemical stability of the material.[26,27]

In this view, the present work aims to synthesize and characterize an adsorbent from agro-industrial residues from a gourd company by carbonization and a chemical activation process for application in the removal of the ASA drug. Moreover, this study carried out equilibrium, kinetic, and thermodynamic studies of adsorption and ecotoxicity assays using saline brine shrimp to evaluate the toxicity of the biochar and the lethal dose of the ASA. The novelty of the study lies in the use of waste from a gourd carving industry as a biosorbent to remove ASA effluent, thus promoting a circular economy, adding value to waste, and meeting the Sustainable Development Goals (SDGs). Furthermore, biochar emerges as a promising biosorbent, transforming organic waste into an eco-efficient solution with high added value for potential application in environmental remediation, redefining the treatment of wastewater with drugs.

2. MATERIALS AND METHODS

2.1. Adsorbate Preparation. The solutions of the ASA commercial (Multilab) were prepared, ranging from 3.3−36.7 mg L^{-1}, and were placed in the ultrasound (Unique-UltraSonic Cleaner model) for 30 min at 50 ± 2 °C.[28]

2.2. Synthesis of the Biochar. For the preparation of the biochar (Figure 1), a slow pyrolysis process was used with *Lagenaria siceraria* waste (local industry, Santa Maria-RS, Brazil). Thus, 30 g of in natura gourd (#20 Mesh Test Sieve − 850 μm) were mixed with 600 mL of 0.1 mol L^{-1} H_3PO_4 (Synth, ACS, 85%) (activating agent) under magnetic stirring (835 rpm/30 min/60 °C).[29] The pH was adjusted (pH 5.5) with 1 mol L^{-1} NaOH (Sigma-Aldrich, PA). Finally, the material was calcined at 600 ± 2 °C with a heating rate of 30 °C min^{-1} for 2 h in a muffle furnace[30] (model EDG, f3000, Brazil). The material was sieved (#100 Mesh Test Sieve − 150 μm).

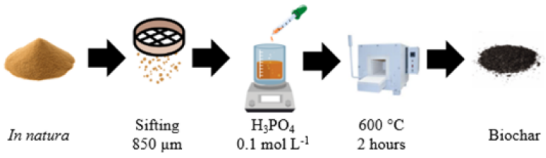

Figure 1. Schematic representation of the biochar synthesis process from *Lagenaria siceraria* waste.

2.3. Adsorption Experiments. 100 mL of the ASA solution (3.3−36.7 mg L^{-1}) were mixed with the biochar (0.08−0.92 g L^{-1}) and pH ranging from 2 to 12, according to the experimental design. The removal of the ASA drug was evaluated by monitoring the process, where aliquots (2 mL) were collected at predetermined times (0, 5, 15, 30, 45, 60, 75, and 90 min). All aliquots collected were filtered (0.22 μm filter, Millex GP) and analyzed by UV−vis spectrophotometer (Shimadzu UV Mini 1240 UV−vis Spectrophotometer-W2B) at the characteristic wavelength of ASA (λ = 327 nm), according to Figure S1 (Supporting Information—SI). Thus, the absorbance was related to the concentration of the ASA through a calibration curve: Abs = 1.048 [ASA] (R^2 = 0.999; N = 7). All tests were performed in duplicate (error value lower than 5%).

The efficiency of the biochar for the ASA removal was evaluated through its adsorption capacity, q_t (mg g^{-1}), according to eq 1,

$$q_t = \frac{(C_0 - C_t)\cdot m}{V} \quad (1)$$

Where C_0 and C_t are the initial and final concentrations of ASA drug in solution (mg L^{-1}), V (L) is the volume of the solution, and m (g) is the mass of the biochar.

2.4. Characterization Techniques. X-ray Diffraction (XRD) was used to check crystallinity in a D2 PHASER XRD diffractometer with a copper tube ($\lambda_{\alpha\text{-Cu}}$ radiation = 0.15418 nm) and an angular range of 10°−70°. Fourier-Transform Infrared Spectroscopy (FTIR) was used to determine the functional groups in a Shimadzu (IR Prestige-21) FTIR Spectrometer (ranging from 3600 to 500 cm^{-1}) with a resolution of 4 cm^{-1}. For the Dynamic Light Scattering (DLS), a NanoBrook Omni (Brookhaven Instrument Corporation, New York, USA) was used with a red laser diode (35 mV, λ = 640 nm) at a detection angle of 90°. The textural properties were determined by N_2 porosimetry using a Micromeritics Gemini VII 2375 Surface Area Analyzer, where the specific surface area (S_{BET}) was determined by the Brunauer−Emmett−Teller equation (BET) method, and the pore diameter and pore volume were carried out by the Barrett−Joyner−Halenda (BJH) method. For the Zeta potential (ZP), a Zetasizer Nano ZS (ZEN3600, UK) with closed capillary cells (DTS 1060) (Malvern Instruments, UK) and a 4 mW He−Ne laser (633 nm) was used. Field Emission Gun Scanning Electron Microscopy (FEG-SEM) was used for morphological analysis with a TESCAN Mira3 XMH Scanning Electron Microscope, with an acceleration voltage of 4 kV and a working distance of 10 mm, with a magnification of 10 kx. The zero charge point (pH_{ZCP}) was determined by the 11-point methodology.[31]

2.5. Experimental Design. The three main factors that influence the process were chosen, such as the concentration of the pollutant (ASA), the adsorbent (Biochar), and pH, based on literature[32,33] were defined by the central composite rotational design (CCRD 2^3) methodology to determine the ideal condition with 3 central points and 6 axial points by using the Gauss−Newton algorithm[34] using the Statistic 10 software

https://doi.org/10.1021/acsomega.5c08131
ACS Omega 2025, 10, 57532−57544

(StatSoft, USA). Table 1 shows the points obtained by CCRD 2^3.

Table 1. Central and Axial Points Were Determined by CCRD.2^3

	−1.67	−1	0	1	+1.67
[ASA] (mg L^{-1})	3.3	10	20	30	36.7
[Biochar] (g L^{-1})	0.08	0.25	0.50	0.75	0.92
pH	2	4	7	10	12

2.6. Equilibrium Adsorption Study. The adsorption equilibrium study relates the availability of active sites on the biosorbent surface with the number of ASA drug molecules, where there are models (isotherms) that describe the adsorption capacity. In this study, the Langmuir[35,36] (eq 2), Freundlich[37−40] (eq 3), Sips[41−43] (eq 4), Toth[44,45] (eq 5), and Khan[46] (eq 6) models were used.

$$q_e = \frac{q_{max}\cdot K_L\cdot C_e}{1 + K_L\cdot C_e} \tag{2}$$

$$q_e = k_F\cdot C_e^{1/n} \tag{3}$$

$$q_e = \frac{q_S\cdot a_S\cdot C_e^{1/S_p}}{1 + a_S\cdot C_e^{1/S_p}} \tag{4}$$

$$q_e = q_{max}\cdot \frac{K_T.\ C_e}{\left(\left(1 + (K_T.\ C_e)^{tn}\right)^{1/tn}\right.} \tag{5}$$

$$q_e = \frac{q_{max}\cdot \alpha_k\cdot C_e}{1 + (K_k\cdot C_e)^{\alpha_k}} \tag{6}$$

Where: q_e is the amount of solute adsorbed per gram of adsorbent at equilibrium (mg g^{-1}); q_{max} the maximum adsorption capacity (mg g^{-1}); K_L is the adsorbent−adsorbate interaction constant (L mg^{-1}); C_e is equilibrium concentration of solute in solution (mg L^{-1}); K_F is the Freundlich adsorption constant ($mg^{1-(1/n)}$ (g^{-1}) $L^{1/n}$); n is the constant related to surface heterogeneity; q_S the monolayer adsorption capacity (mg g^{-1}); a_S the Sips isotherm model constant (L g^{-1}); S_P the Sips isotherm exponent; K_T is Toth isotherm constant (L mg^{-1}); tn is a constant dimensionless associated with the heterogeneity of the adsorbent surface; K_k the Khan isotherm model constant (L mg^{-1}) and α_k is Khan isotherm model exponent.

2.7. Adsorption Kinetics. Kinetic studies on the adsorption of solutes from aqueous solutions are applied to determine how fast the process occurs or at what rate equilibrium is reached.[47] Thus, the best conditions of biochar concentration and pH value were fixed, while varying the ASA concentration (5, 10, 30, 50 mg L^{-1}). Moreover, pseudo first-order (PFO),[48] pseudo second-order (PSO),[49,50] and intraparticle diffusion-adsorption models (ID)[51] were used, according to the eqs 7−89, respectively.

$$q_t = q_1\cdot(1 - e^{-k_1 t}) \tag{7}$$

$$q_t = \frac{t}{\left(\frac{1}{k_2\cdot q_2^2}\right) + \left(\frac{t}{q_2}\right)} \tag{8}$$

$$q_t = k_{id}\cdot t^{0.5} + C \tag{9}$$

Where: k_1 (min^{-1}) is the rate constant of pseudo-first-order; q_1 (mg g^{-1}) is the value of adsorption capacity for PFO; k_2 (g mg^{-1} min^{-1}) is the rate constant of pseudo-second-order; q_2(mg g^{-1}) is the value of adsorption capacity for PSO; k_{id} is the intraparticle diffusion rate constant (mg g^{-1} $min^{-0.5}$); and C reflects the effect of the boundary layer or surface adsorption (mg g^{-1}).

2.8. Adsorption Thermodynamics. Thermodynamic parameters were determined by the changes in Gibbs free energy (ΔG^0, kJ mol^{-1}), entropy (ΔS^0, kJ mol^{-1} K^{-1}), and enthalpy (ΔH^0, kJ mol^{-1}), which indicate whether the process is spontaneous, exothermic, or endothermic[52] (eqs 10−12).

$$\Delta G^0 = -R\cdot T\cdot \ln K_c \tag{10}$$

$$\ln K_c = \frac{\Delta S^0}{R} - \frac{\Delta H^0}{RT} \tag{11}$$

$$K_c = \frac{q_e}{C_e} \tag{12}$$

Where: K is the equilibrium constant (L gK_c^{-1}); q_e is the amount of solute adsorbed per gram of adsorbent at equilibrium (mg g^{-1}); C_e is the concentration in solution (mg L^{-1}); T is absolute temperature (298.15, 308.15, and 318.5 K); and R is the universal gas constant (8.314 J mol^{-1} K^{-1}).

2.9. Statistical Analysis. The kinetic and equilibrium parameters were determined by fitting the models to the data using nonlinear regression, using the Statistic 10 software (StatSoft, USA) with the Quasi-Newton method. The coefficient of determination (R^2), adjusted coefficient of determination (R^2_{adj}), root-mean-square error (RMSE), the sum of squared errors (SSE), and average relative error (ARE) were used to evaluate the model's fit quality, according to eqs 13−14151617):[53−56]

$$R^2 = 1 - \frac{\sum_{i=1}^{N}(q_{exp} - q_{pred})^2}{\sum_{i=1}^{N}\left(q_{exp} - \hat{q}_{pred}\right)^2} \tag{13}$$

$$R^2_{adj} = 1 - \left[\frac{(1 - R^2)\cdot(n - p)}{(n - p - 1)}\right] \tag{14}$$

$$RMSE = \sqrt{\frac{\sum_{i=1}^{N}\left(q_{exp} - \hat{q}_{pred}\right)^2}{n}} \tag{15}$$

$$SSE = \frac{1}{n}\cdot\sum_{1}^{n}(q_{exp} - q_{pred})^2 \tag{16}$$

$$ARE = \frac{1}{n}\cdot\sum_{1}^{n}\frac{(q_{exp} - q_{pred})}{q_{exp}} \tag{17}$$

Where: q_{exp} and $\hat{q}_{pred}$ are the experimental and the predicted adsorption capacity (mg g^{-1}), respectively; $\hat{q}_{pred}$ is the predicted data associated with the response (absorbance); n is the number of data; p is the number of model parameters.

2.10. Ecotoxicity Tests. *2.10.1. Preparation of Artificial Saline Water.* For the preparation of artificial saline water, 1 L

https://doi.org/10.1021/acsomega.5c08131
ACS Omega 2025, 10, 57532−57544

of distilled water was mixed with 23 g of NaCl (Synth), 11 g of $MgCl_2{\cdot}6H_2O$ (Synth), 4 g of Na_2SO_4 (Nuclear), 1.3 g of $CaCl_2{\cdot}2H_2O$ (Nuclear), and 0.7 g of KCl (Synth). Moreover, the pH of the solution was adjusted to 9 with a solution of Na_2CO_3 (Synth),[57] which was measured using a benchtop pH meter (Ohaus pH Meter Model ST3100-F).

2.10.2. Cyst Eclosion and Incubation Procedure. For the hatching of the cysts, a 1 L beaker was used, to which 500 mL of artificial saline water was added. The beaker was protected with aluminum foil, leaving only a small opening on the upper surface, and illuminated by an 18 W lamp at a distance of about 30 cm. The water was aerated for 15 min and then added 10 mg of *Artemia salina* cysts where the aeration was maintained throughout the hatching process using a commercial aquarium pump for 48 h with a flow rate of 3.5 L min^{-1} in a controlled temperature environment of 28 ± 2 °C, a salinity of 32 $\mu g\ mL^{-1}$ and a pH 9.[58]

2.10.3. Acute Toxicity and Lethal Concentration. For the determination of acute toxicity and lethal concentration (L_C), a negative control (NC) was prepared, consisting of artificial saline water without any extra substance, and the positive control (PC) consisted of copper sulfate solution ($CuSO_4$, 0.0006 mg mL^{-1}) and finally the biochar concentrations ranged from 100 to 1000 mg L^{-1} and the ASA concentrations ranged from 50 to 350 mg L^{-1}.[59]

Thus, the assays were carried out in triplicate in test tubes containing 10 mL of the test or control solution with 10 nauplii at 28 ± 2 °C for 48 h with a 12 h light/12 h dark photoperiod. Afterward, the dead nauplii or any signs of abnormal behavior (e.g., difficulty in swimming[60] were counted.

3. RESULTS AND DISCUSSION

3.1. Characterization. Figure 2 shows the XRD diffractograms of the *in natura* gourd and biochar, where crystalline

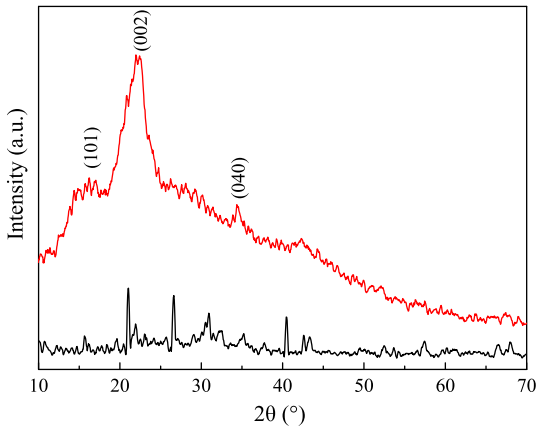

Figure 2. XRD pattern diffractograms of *in natura* gourd waste and biochar.

peaks were identified: at 16.19° (101), 22.42° (002), and 34.67° (040), indicating the presence of hemicellulose, lignin, and cellulose,[61] which disappear or reduce in intensity with the pyrolysis process in the development of biochar. Moreover, due to the calcination process (600 °C), the reactivity of phosphorus increases, forming possible functional groups on the surface of the biochar and allowing the formation of crystalline phases.[62] It is worth noting that this is important for the adsorption of the pollutant, as the crystalline phase can

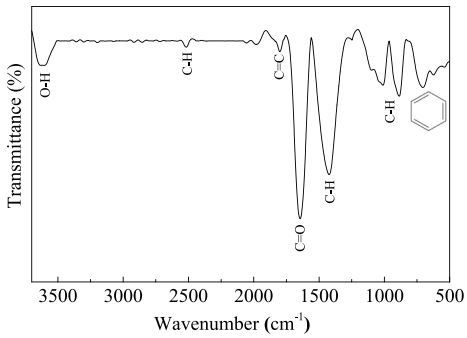

Figure 3. FTIR spectrum of biochar from *Lagenaria siceraria* waste.

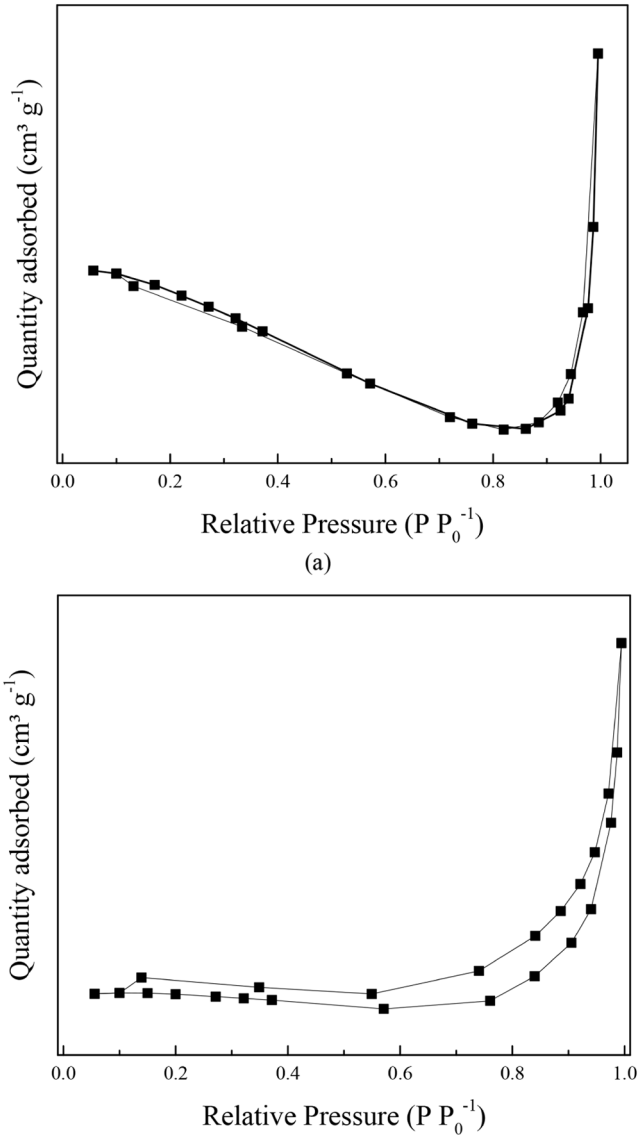

Figure 4. (a) N_2 adsorption/desorption isotherms of (a) *in natura* gourd waste and (b) biochar.

maintain an organized structure, while the amorphous phase promotes more empty spaces to accommodate the ASA molecules, allowing an increase in diffusive stages (extra- and intraparticle), as well as mass transfer phenomena.

https://doi.org/10.1021/acsomega.5c08131
ACS Omega 2025, 10, 57532−57544

Table 2. Specific Surface Area (S_{BET}), Pore Diameter (D_p), Pore Volume (V_p), and Zeta Potential (ZP) of the *In Natura* Gourd Waste and Biochar

	S_{BET} (m^2 g^{-1})	D_p (nm)	V_p (cm^3 g^{-1})	ZP (mV)
In natura	0.09 ± 0.04	78.3 ± 2.07	0.002 ± 0.01	-19.96 ± 0.52
Biochar	0.35 ± 0.01	36.3 ± 9.77	0.002 ± 0.01	-18.76 ± 8.05

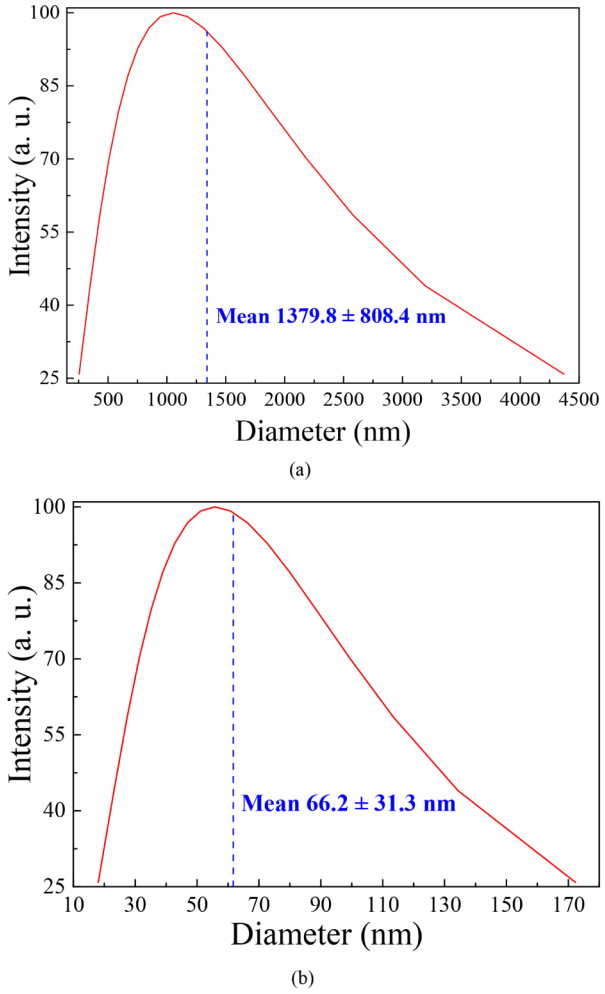

Figure 5. Distribution of particle size obtained from the DLS analysis for (a) *in natura* gourd waste and (b) biochar.

Figure 3 illustrates the FTIR spectrum of the biochar, where several key absorption bands can be identified:[63−69] (a) at 3600 cm^{-1} are assigned to the stretching vibration of O−H bonds relative to alcohols, carboxylic acids, phenols, or hydroxyl functional groups; (b) at 2500 cm^{-1} and 1430 cm^{-1} correspond to the C−H vibrational modes of methyl groups; (c) at 1800 cm^{-1} originate from either the C =O stretching vibration of carbonyl-related structures or the C−O vibration of carboxylic groups; (d) at 1685 cm^{-1} the axial stretching of − C= ; (e) C associated with −C−H (alkene and alkenyl side chains) in the region of 990 cm^{-1}; and (f) the formation of an aromatic ring in the region of 750 cm^{-1}.

Figures 4(a) and 4(b) represent the N_2 adsorption/desorption isotherms of the *in natura* gourd and biochar, respectively. According to Figure 4(a), the biochar represents a type III isotherm, describing an adsorption process on macroporous adsorbents with strong and weak adsorbate-adsorbent interactions, respectively, while Figure 4(b) presents a type V isotherm with hysteresis type H3, which means that

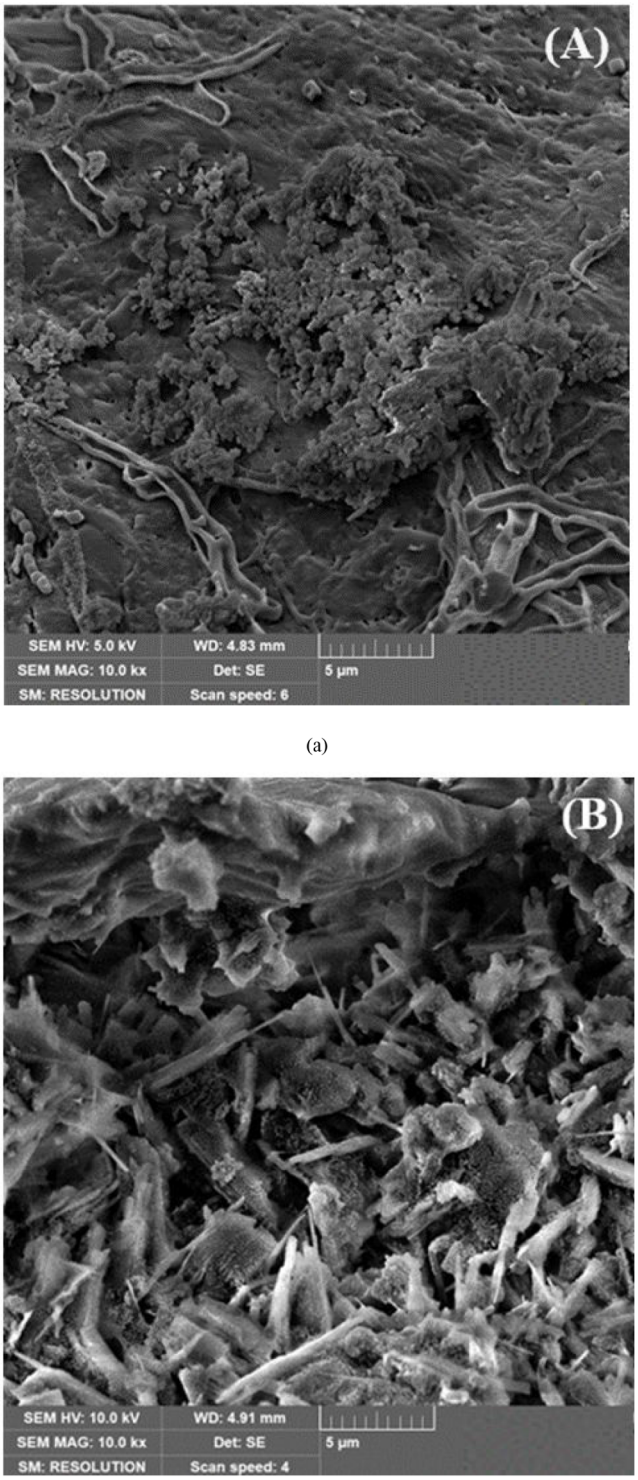

Figure 6. FEG-SEM micrographs with 10 kx magnification for (a) *in natura* gourd waste and (b) biochar.

https://doi.org/10.1021/acsomega.5c08131
ACS Omega 2025, 10, 57532−57544

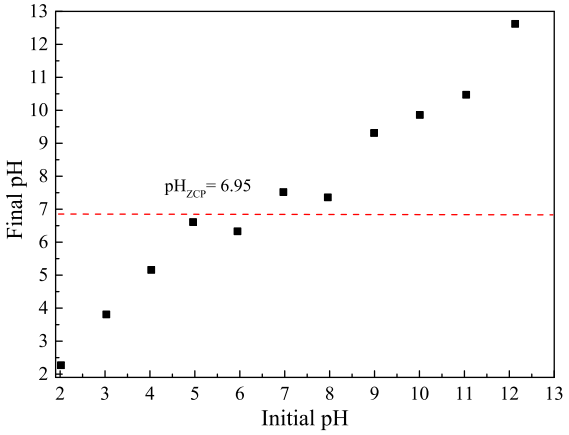

Figure 7. Zero charge point (pH$_{ZCP}$) of the biochar from the *Lagenaria siceraria* waste.

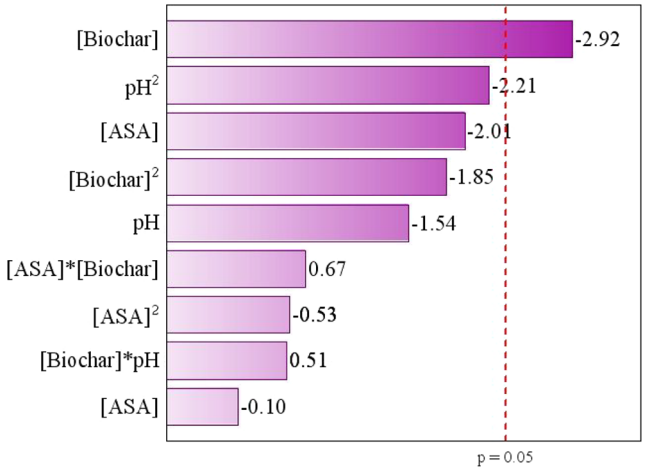

Figure 8. Pareto chart from CCRD 2^3 for the removal of the ASA drug.

Table 3. Sum of Squares (SS), Degrees of Freedom (df), Mean Square Error (MS), F_{cal} (calculated Degrees of Freedom), F_{tab} (degrees of Freedom Tabulated), and Determination Coefficient (R^2) for ASA Adsorption

	SS	df	MS	F_{cal}	F_{tab}	R^2
[ASA]	707.844	1	707.844	325	3.68	0.7613
[ASA]^2	51.153	1	51.153			
[biochar]	1487.127	1	1487.127			
[biochar]^2	600.278	1	600.278			
pH	413.267	1	413.267			
pH^2	858.754	1	858.754			
[ASA] * [biochar]	78.438	1	78.438			
[ASA] * pH	1.892	1	1.892			
[biochar] * pH	45.840	1	45.840			
Error	1222.786	7	174.684			
Total SS	5122.47409	16	–			

the material is mesoporous, with pores that are cracks between aggregated particles or lamellar structures.[70,71]

In addition, the physical properties after the carbonization process of *in natura* material are shown in Table 2, indicating an increase in S_{BET} and V_p due to the removal of inorganic compounds, which were initially added to prevent the

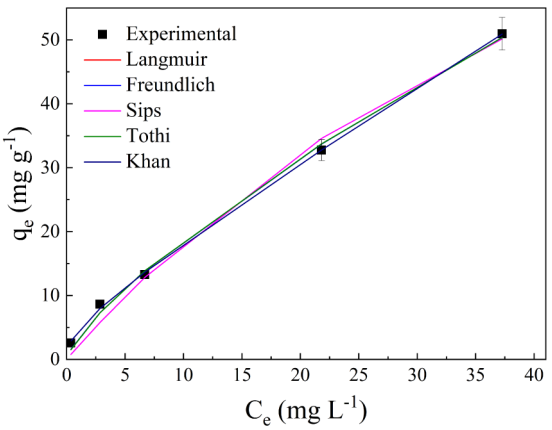

Figure 9. Equilibrium adsorption curves for adsorption of ASA drug onto biochar (biochar concentration = 0.25 g L^{-1} and pH 4).

expansion or shrinkage of carbon molecules in the adsorbent during the carbonization and activation process. Moreover, the mesoporosity of materials can be confirmed by the values of the average pore diameter of these materials.[72,73] Regarding ZP, all materials showed a negative charge due to the presence of carboxylic groups originating from hemicellulose, lignin, and cellulose in the *in natura* gourd waste.[74] According to the DLS results (Figure 5), the average size of the agglomerated particles showed a significant reduction (from 1379.8 to 66.2 nm), indicating the colloidal stability of the biochar due to the thermal process (calcination) during its synthesis, which contributes to the adsorption process by providing greater availability of contact area between the biosorbent surface and the ASA drug.

Figure 6 (a) and (b) presents the morphology of the materials through FEG-SEM micrographs of the *in natura* gourd waste and biochar, respectively. Figure 6(a) shows the morphology of the *in natura* with a disorganized structure without visible pores that contains fibers typically found in biomasses, while for biochar (Figure 6(b) showed a porous network structure is shown due to the activation and carbonization process, being an extremely suitable morphology for dye adsorption as it promotes the access of the ASA molecules to the internal structure of the adsorbent.[75]

Figure 7 shows the pH$_{ZCP}$ of the biochar, which was 6.95, as found in the literature.[76] When the pH of the solution is lower than this pH$_{ZCP}$, it indicates that the surface of the biochar was protonated, thus aiding in the adsorption of negatively charged molecules (presence of carboxylic groups), and many anions were adsorbed to balance the positive charges. Otherwise, the adsorption process can be explained by the electrostatic attraction between the charge present in the adsorbent and the anionic group in the solution.[77]

3.2. Experimental Design. Figure 8 shows the Pareto chart for ASA removal, indicating that the independent variable affecting the adsorption process for removing the ASA drug was the concentration of biochar. Thus, the linear interaction of biochar concentration had a negative direct effect due to the electrostatic interactions and the selective interactions of the active sites available with the ASA molecules. Therefore, the ideal conditions for ASA removal by adsorption were 10 mg L^{-1} of ASA, 0.25 g L^{-1} of biochar, and pH 4.

Table 3 shows the variance analyses (ANOVA) of the experimental design for ASA removal, where the main parameters and regression coefficients are denoted, resulting

https://doi.org/10.1021/acsomega.5c08131
ACS Omega 2025, 10, 57532−57544

Table 4. Equilibrium Parameters for the Adsorption of ASA Drug onto Biochar

Parameter	Value	R^2	R^2_{adj}	SSE	ARE (%)	RMSE
Langmuir						
q_{max} (mg g^{-1})	137.33 ± 6.87	0.990	0.981	3.114	22.771	1.764
K_L (L mg^{-1})	0.0154 ± 0.001					
Freundlich						
K_F ($mg^{1-(1/n)}$) (g^{-1}) L1/n)	3.33 ± 0.17	0.997	0.995	0.875	12.639	0.936
n	1.33 ± 0.07					
Khan						
q_{max} (mg g^{-1})	3.09 ± 0.15	0.999	0.999	0.136	4.562	0.369
K_K	40.88 ± 2.04					
a_K	0.34 ± 0.01					
Sips						
q_s (mg g^{-1})	137.35 ± 6.87	0.990	0.981	3.114	22.713	1.764
a_S (L g^{-1})	1.016 ± 0.05					
S_P	65.82 ± 3.29					
Toth						
q_{max} (mg g^{-1})	0.015 ± 0.001	0.997	0.994	0.916	13.004	0.957
K_T (L mg^{-1})	9861.97 ± 493.1					
t_n	0.26 ± 0.01					

Table 5. Kinetic Parameters for the Adsorption of ASA Drug onto Biochar

[ASA] (mg L^{-1})	q_1 (mg g^{-1})	k_1 (min^{-1})	R^2	R^2_{adj}	SSE	ARE (%)	RMSE
Pseudo first-order model (PFO)							
1	2.555 ± 0.128	3.321 ± 0.166	0.974	0.970	4×10^{-17}	2×10^{-8}	6×10^{-9}
5	8.839 ± 0.442	0.360 ± 0.018	0.818	0.788	0.086	0.321	0.293
10	18.056 ± 0.903	0.022 ± 0.001	0.919	0.905	0.096	0.245	0.310
30	28.636 ± 1.432	18.213 ± 0.911	0.485	0.399	3×10^{-22}	5×10^{-12}	1×10^{-11}
50	45.173 ± 2.259	19.924 ± 0.996	0.552	0.477	1×10^{-18}	2×10^{-10}	1×10^{-9}
Pseudo second-order model (PSO)							
[ASA] (mg L^{-1})	q_2 (mg g^{-1})	k_2 (g (mg $min)^{-1}$)	R^2	R^2_{adj}	SSE	ARE (%)	RMSE
1	2.555 ± 0.128	9×10^{-4} ± 0.001	0.974	0.970	0.013	0.434	0.117
5	8.881 ± 0.444	0.187 ± 0.009	0.779	0.766	0.085	0.320	0.291
10	26.413 ± 1.321	6×10^{-4} ± 0.001	0.916	0.902	0.335	0.592	0.578
30	37.314 ± 1.866	3×10^{-3} ± 0.001	0.783	0.747	0.389	0.209	0.624
50	58.764 ± 2.938	2×10^{-3} ± 0.001	0.864	0.841	1.089	0.222	1.043
Intraparticle diffusion model (IDM)							
[ASA] (mg L^{-1})	C (mg g^{-1})	k_{id} (mg g^{-1} min−1/2)	R^2	R^2_{adj}	SSE	ARE (%)	RMSE
1	1.301 ± 0.065	0.169 ± 0.008	0.371	0.266	0.058	0.914	0.242
5	3.945 ± 0.197	0.651 ± 0.033	0.391	0.290	6×10^{-22}	2×10^{-11}	2×10^{-11}
10	1.351 ± 0.068	1.840 ± 0.092	0.893	0.875	0.066	0.268	0.258
30	6.239 ± 0.312	3.406 ± 0.170	0.596	0.528	5×10^{-15}	2×10^{-8}	7×10^{-8}
50	9.621 ± 0.481	5.414 ± 0.271	0.688	0.636	6×10^{-22}	4×10^{-12}	2×10^{-11}

in a predicted model with an F_{cal} of 325 and an F_{tab} of 3.68, indicating 76.13% of the adjusted experimental data. The R^2 was 0.7613, possibly due to the material tending to agglomerate, which does not make the linear model predictable and can generate some prediction errors, thus decreasing the R^2 value.

3.3. Adsorption Isotherms. The experimental data were fitted with Langmuir, Freundlich, Khan, Sips, and Toth adsorption isotherm models, according to Figure 9. The corresponding model parameters are listed in Table 4.

According to Figure 9 and Table 4, the Khan model was the best fit for the experimental data, as shown in Figure 9 (R^2 and R^2_{adj} = 0.999), since this model generated lower error values (SSE, ARE, and RMSE) than the other isotherms tested. The Khan isotherm is particularly notable for its hybrid nature, incorporating characteristics of both the Langmuir and Freundlich models. It describes adsorption as occurring simultaneously in monolayer and multilayer forms. This implies that adsorption begins with a strong interaction at specific active sites (akin to the Langmuir model) but transitions to multilayer adsorption as the surface becomes saturated, driven by weaker adsorbate−adsorbate interactions (similar to the Freundlich model). This dual mechanism makes the Khan model especially suitable for systems where heterogeneous adsorption occurs due to a combination of surface site specificity and adsorbent interactions.[79]

3.4. Adsorption Kinetics. Table 5 shows the parameters evaluated from ASA adsorption kinetic studies, and Figure 10 shows the curve of each evaluated kinetic model. Thus, the ASA molecules' adsorption onto the biochar surface occurred

https://doi.org/10.1021/acsomega.5c08131
ACS Omega 2025, 10, 57532−57544

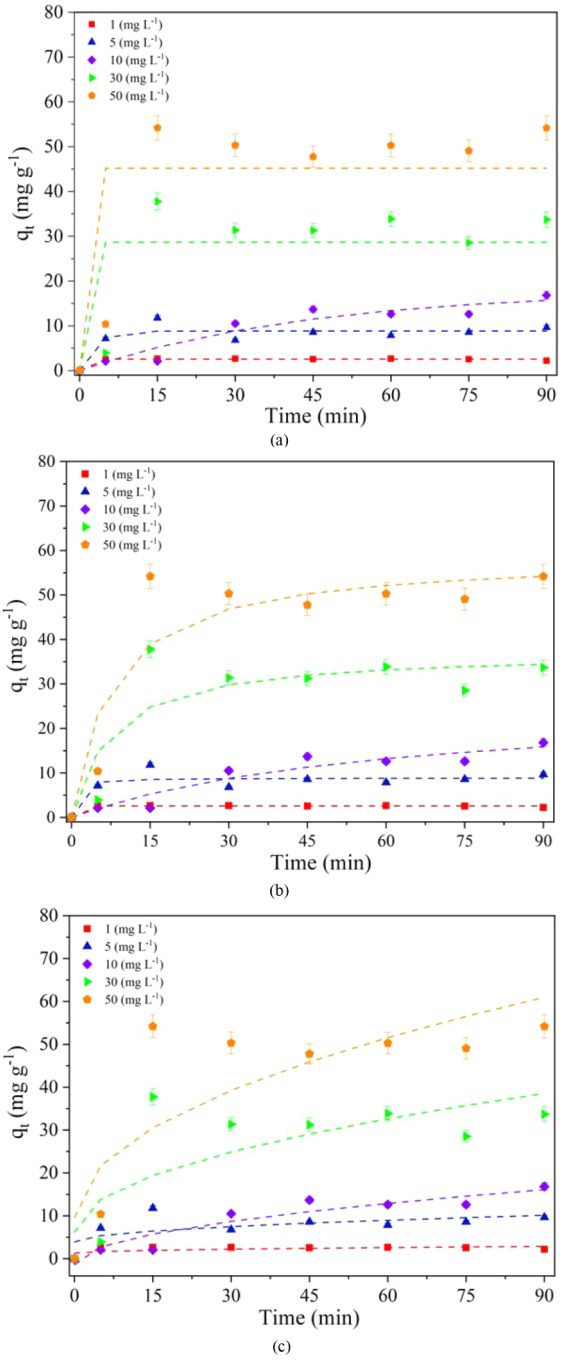

Figure 10. Kinetic curves for the ASA drug onto biochar of (a) PFO, (b) PSO, and (c) IDM (biochar concentration = 0.25 g L^{-1} and pH 4).

Table 6. Thermodynamic Parameters for the Adsorption of ASA Drug onto Biochar

T (K)	K_c (L g^{-1})	ΔG^0 (kJ mol^{-1})	ΔH^0 (kJ mol^{-1})	ΔS^0 (kJ mol^{-1} K^{-1})
298.15	2.08	−1.8	27.38	0.09
308.15	3.14	−2.8		
318.15	4.16	−3.8		

fast within the first 15 min, and the rate gradually decreased until equilibrium, due to the reduction of unoccupied adsorption sites and the decrease in the concentration gradient.

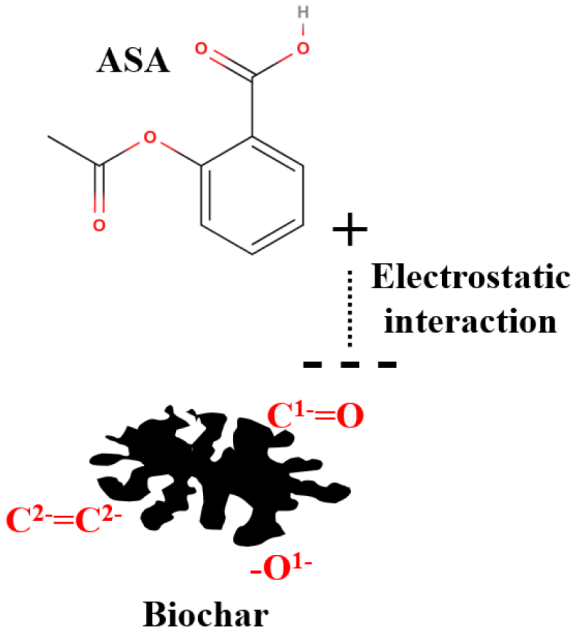

Figure 11. ASA adsorption mechanism using biochar from *Lagenaria siceraria* waste.

As we can see in Table 5, the kinetic evaluation revealed that, at low ASA concentrations (1−10 mg L^{-1}), the pseudo first-order (PFO) model presented the best fit (R^2 > 0.81), indicating a predominance of fast adsorption at surface sites and physical interactions. At higher concentrations (30−50 mg L^{-1}), the pseudo second-order (PSO) model was more adequate (R^2 up to 0.864), suggesting an increasing contribution of specific chemical interactions at higher-energy sites. The intraparticle diffusion model (IDM), although presenting good correlation coefficients (R^2 > 0.89), did not explain the process alone, indicating that internal diffusion acts in conjunction with surface phenomena. Thus, ASA adsorption follows a multiphase mechanism, dependent on the concentration and availability of active sites. The PSO model is based on the premise that the adsorption rate is proportional to the square of the amount of adsorbate still available, implying a stronger dependence on specific interactions and the limited availability of active sites.[77] Figure 10 shows the plot of the studied kinetic models: (a) PFO, (b) PSO, and (c) IDM.

3.5. Adsorption Thermodynamics. Table 6 shows the values obtained in the thermodynamic study. ΔS^0, when positive, indicates an increase in the entropy of the process. A positive ΔH indicates an endothermic process, thus absorbing heat. Furthermore, the magnitude of ΔH^0 indicates how the adsorbent interacts with the adsorbate. This interaction occurred by physisorption through van der Waals forces.[78] Typically, ΔH^0 values are less than 20 (kJ mol^{-1}), which was previously confirmed in the kinetic study at the same ASA concentration, and ΔG^0, which has negative energy, indicates that the process occurs spontaneously.

Operational conditions: [ASA] = 10 mg L^{-1} | [Biochar] = 0.25 g L^{-1} | pH = 4|.

3.6. Adsorption Mechanism. It was possible to identify the type of adsorption that occurs in the process, identifying the best equilibrium model, which was the Khan isotherm. This model indicates a combination of both Langmuir and Freundlich, suggesting that adsorption can occur in a hybrid form as a monolayer and multilayer.[80] In kinetics, lower

https://doi.org/10.1021/acsomega.5c08131
ACS Omega 2025, 10, 57532−57544

Table 7. Adsorption Capacities of Biochar for ASA and Other Organic Pollutants

Modification method	Biochar feedstock	Temperature (°C)	Pollutant	q_{max} (mg g^{-1})	Removal mechanism
Acid bath (H_3PO_4)	Sawdust gourd	600	ASA	137	Electrostatic interaction
N doping (KOH NaN3)[84]	Corn stalks	700	Atrazine	104	π-π EDA Hydrophobic effect
Biological modification[85] (*Arthrobacter sp.* ZXY-2 *Aspergillus niger* Y3)	Maize straw	700	Atrazine	103	π-π EDA Hydrophobic effect
Acid bath Microwave (H_3PO_4)[86]	Plantain Leaf	110	Malachite green	266	π-π EDA H-bonding Electrostatic interaction
Pyrolysis with N_2[87]	Rice straw	500	Methylene blue	50	π-π EDA Electrostatic interaction
Corn cob ($ZnCl_2$)[88]	Corn cob	700	Amoxicillin	175	n-π interactions hydrogen bonding

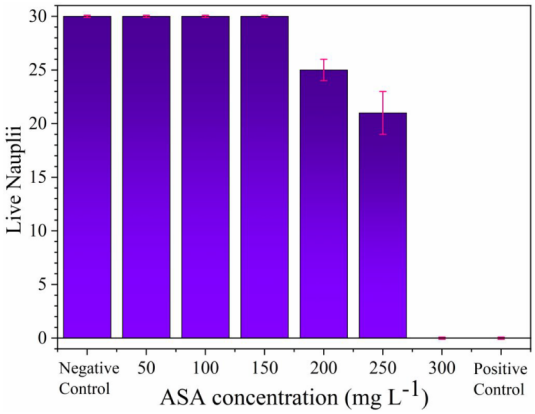

Figure 12. Ecotoxicity tests performed with *Artemia salina* .

Table 8. Assessment of Acute Toxicity of ASA after 48 h in Different Organisms

Organisms	LD_{50} (mg L^{-1})	Reference
Daphnia magna	310	89
Ceriodaphnia silvestrii	69	90
Daphnia	88	91
Daphnia magna	136	92
Artemia sp.	305	93
Artemia Salina	264	In this study

concentrations (1, 5, and 10 mg L^{-1}) had a better fit for PFO, suggesting physical adsorption, while higher values (30 and 50 mg L^{-1}) had a better fit for PSO, suggesting chemical adsorption.[81] Finally, with the thermodynamic study, ΔH^0 was lower than 20 kJ mol^{-1}, indicating adsorption with weak forces (van der Waals) that is physical.[82,83] Therefore, the adsorption occurred predominantly in a physical way by electrostatic action, interacting with the surface of the biochar that adsorbed the ASA in a multilayer and monolayer hybrid, according to Figure 11. Table 7 shows that adsorption mechanisms vary according to the modification method and the type of pollutant. In the present study, gourd biochar treated with H_3PO_4 exhibited ASA removal predominantly through electrostatic interactions, which was attributed to the presence of oxygenated functional groups capable of modulating the surface charge. In contrast, other studies have reported mechanisms based on π–π electron donor–acceptor (EDA) interaction and hydrophobic effects (atrazine and methylene blue), associated with the high aromaticity of biochar at high temperatures, or even on hydrogen bonds (malachite green and amoxicillin), favored by polar groups of the adsorbates. These results highlight that acid modification directs adsorption toward electrostatic processes, distinguishing it from other reported mechanisms and reinforcing selectivity against ionizable pollutants.

3.7. Ecotoxicity Tests. Figure 12 shows the results obtained from the ecotoxicity tests, where ASA exhibited signs of toxicity at a concentration of 200 mg L^{-1}. Shortly thereafter, the lethal dose 50% (L_{D50}) was approximately 264 mg L^{-1}, concentrations above 300 mg L^{-1} resulted in a lethal dose of 100% (L_{D100}). For the biochar toxicity tests, within the range of 100–1000 mg L^{-1}, the adsorbent demonstrated no toxicity to *Artemia salina*.

Table 8 shows the acute (48 h) toxicity results of ASA for different test organisms, revealing a significant difference in sensitivity between species. The freshwater cladoceran *Ceriodaphnia silvestrii* was the most sensitive, presenting an LD_{50} value of 69 mg L^{-1}, followed by *Daphnia sp.* with 88 mg L^{-1}. For *Daphnia magna*, LD_{50} values ranged from 136 to 310 mg L^{-1}, indicating possible variations between strains or experimental conditions. The marine organisms *Artemia salina* (264 mg L^{-1}) and *Artemia* sp. (305 mg L^{-1}) showed the lowest sensitivities, suggesting greater resistance to the drug compared to that of cladocerans. These data support the idea that ASA toxicity varies by species and that freshwater organisms, especially of the genus *Ceriodaphnia*, may be more vulnerable to this emerging contaminant in aquatic environments.

4. CONCLUSION

In the present study, it was possible to develop and characterize a novel biochar from *Lagenaria siceraria* waste, as well as to determine the ideal adsorption process conditions for ASA removal (10 mg L^{-1} of ASA, 0.25 g L^{-1} of biochar, and pH 4). The adsorption isotherm data showed an excellent fit with the Khan isotherm model (R^2 = 0.999), which indicates a hybrid adsorption mechanism involving both monolayer and multilayer adsorption. Kinetic analysis revealed that the PFO model provided the best fit (R^2 = 0.974) under most conditions, indicating that the adsorption process is predominantly controlled by physical interactions, such as van der Waals forces and electrostatic attractions. The enthalpy change ΔH^0 values were consistently below 20 kJ mol^{-1}, characteristic of physical adsorption mechanisms, while the negative ΔG values confirmed the spontaneity of the adsorption process. Ecotoxicity tests using *Artemia salina* revealed that ASA exhibited a lethal dose (LD50) at 300 mg L^{-1}, indicating moderate toxicity in aquatic environments. In contrast, biochar showed no measurable toxicity within the tested concentration range of 100–1000 mg L^{-1}. Therefore, the novel biochar demonstrated excellent performance for ASA removal under various conditions, showing strong adsorption capacity,

https://doi.org/10.1021/acsomega.5c08131
ACS Omega 2025, 10, 57532–57544

temperature resilience, and environmental safety. These results position biochar as a sustainable and cost-effective alternative for the remediation of organic pollutants in water, with potential applications in wastewater treatment systems and environmental protection initiatives.

■ ASSOCIATED CONTENT

Data Availability Statement

The data underlying this study are available in the published article and its online Supporting Information.

Supporting Information

The Supporting Information is available free of charge at https://pubs.acs.org/doi/10.1021/acsomega.5c08131.

Additional experimental details, materials, and experimental design, including the UV−vis scanning of the ASA drug, the calibration curve of the ASA drug, and CCRD 2^3 results (PDF)

■ AUTHOR INFORMATION

Corresponding Author

William Leonardo da Silva − *Applied Nanomaterials Research Group (GPNAp), Franciscan University (UFN), Santa Maria, RS 97010-032, Brazil;* orcid.org/0000-0002-7804-9678; Email: Williamleonardo_silva@hotmail.com

Authors

Matheus Londero da Costa − *Applied Nanomaterials Research Group (GPNAp), Franciscan University (UFN), Santa Maria, RS 97010-032, Brazil*

Leandro Rodrigues Oviedo − *Applied Nanomaterials Research Group (GPNAp), Franciscan University (UFN), Santa Maria, RS 97010-032, Brazil*

Giovani Pavoski − *Polytechnical School of Chemical Engineering University of the Sao Paulo (USP), São Paulo, SP 05508-010, Brazil*

Jorge Alberto Soares Tenório − *Polytechnical School of Chemical Engineering University of the Sao Paulo (USP), São Paulo, SP 05508-010, Brazil*

Denise Crocce Romano Espinosa − *Polytechnical School of Chemical Engineering University of the Sao Paulo (USP), São Paulo, SP 05508-010, Brazil*

Yolice Patricia Moreno − *Strategic Technologies Center of Northeast (CETENE), Recife, PE 50740-545, Brazil; Department of Fundamental Chemistry (DQF), Federal University of Pernambuco (UFPE), Recife, PE 50670-901, Brazil*

Daniel Moro Druzian − *Applied Nanomaterials Research Group (GPNAp), Franciscan University (UFN), Santa Maria, RS 97010-032, Brazil*

Sthéfany Nunes Loureiro − *Applied Nanomaterials Research Group (GPNAp), Franciscan University (UFN), Santa Maria, RS 97010-032, Brazil*

Complete contact information is available at: https://pubs.acs.org/10.1021/acsomega.5c08131

Funding

The Article Processing Charge for the publication of this research was funded by the Coordenacao de Aperfeicoamento de Pessoal de Nivel Superior (CAPES), Brazil (ROR identifier: 00x0ma614).

Notes

The authors declare no competing financial interest.

■ ACKNOWLEDGMENTS

University of São Paulo (LAREX, USP), Federal University of Pernambuco (Department of Fundamental Chemistry, UFPE), and Franciscan University (UFN) for their support and assistance in carrying out the present work.

■ REFERENCES

(1) Santos-Gallego, C. G.; Badimon, J. Overview of Aspirin and Platelet Biology. *Am. J. Cardiol.* **2021**, *144*, S2−S9.

(2) Kowalska, M.; Woźniak, M.; Kijek, M.; Mitrosz, P.; Szakiel, J.; Turek, P. Management of Validation of HPLC Method for Determination of Acetylsalicylic Acid Impurities in a New Pharmaceutical Product. *Sci. Rep.* **2022**, *12* (1), 1−10.

(3) Mohanta, M.; Thirugnanam, A. Development of Multifunctional Commercial Pure Titanium-Polyethylene Glycol Drug-Eluting Substrates with Enhanced Optical and Antithrombotic Properties. *Cardiovasc. Eng. Technol.* **2023**, *14*, 37−51.

(4) Parolini, M. Toxicity of the Non-Steroidal Anti-Inflammatory Drugs (NSAIDs) Acetylsalicylic Acid, Paracetamol, Diclofenac, Ibuprofen and Naproxen towards Freshwater Invertebrates: A Review. *Sci. Total Environ.* **2020**, *740*, 140043.

(5) Magina, S.; Barros-Timmons, A.; Ventura, S. P. M.; Evtuguin, D. V. Evaluating the Hazardous Impact of Ionic Liquids − Challenges and Opportunities. *J. Hazard. Mater.* **2021**, *412*, 125215−125241.

(6) Albendín, M. G.; Aranda, V.; Coello, M. D.; González-Gómez, C.; Rodríguez-Barroso, R.; Quiroga, J. M.; Arellano, J. M. Pharmaceutical Products and Pesticides Toxicity Associated with Microplastics (Polyvinyl Chloride) in Artemia Salina. *Int. J. Environ. Res. Public Health* **2021**, *18* (20), 10773−10798.

(7) Gong, Y.; Zhang, K.; Geng, N.; Wu, M.; Yi, X.; Liu, R.; Challis, J. K.; Codling, G.; Xu, E. G.; Giesy, J. P. Molecular Mechanisms of Zooplanktonic Toxicity in the Okadaic Acid-Producing Dinoflagellate Prorocentrum Lima. *Environ. Pollut.* **2021**, *279*, 116942−116952.

(8) Tominaga, F. K.; Silva, T. T.; Boiani, N. F.; de Jesus, J. M. S.; Teixeira, A. C. S. C.; Borrely, S. I. Is Ionizing Radiation Effective in Removing Pharmaceuticals from Wastewater? *Environ. Sci. Pollut. Res.* **2021**, *28* (19), 23975−23983.

(9) Teodosiu, C.; Gilca, A.-F.; Barjoveanu, G.; Fiore, S. Emerging Pollutants Removal through Advanced Drinking Water Treatment: A Review on Processes and Environmental Performances Assessment. *J. Cleaner Prod.* **2018**, *197*, 1210−1221.

(10) Tobajas, M.; Verdugo, V.; Polo, A. M.; Rodriguez, J. J.; Mohedano, A. F. Assessment of Toxicity and Biodegradability on Activated Sludge of Priority and Emerging Pollutants. *Environ. Technol.* **2016**, *37* (6), 713−721.

(11) Muraro, P. C. L.; Mortari, S. R.; Vizzotto, B. S.; Chuy, G.; dos Santos, C.; Brum, L. F. W.; da Silva, W. L. Iron Oxide Nanocatalyst with Titanium and Silver Nanoparticles: Synthesis, Characterization and Photocatalytic Activity on the Degradation of Rhodamine B Dye. *Sci. Rep.* **2020**, *10* (1), 1−9.

(12) Hilal, N.; Wright, C. J. Exploring the Current State of Play for Cost-Effective Water Treatment by Membranes. *Npj Clean Water* **2018**, *1* (1), 8−12.

(13) Quesada, H. B.; Baptista, A. T. A.; Cusioli, L. F.; Seibert, D.; de Oliveira Bezerra, C.; Bergamasco, R. Surface Water Pollution by Pharmaceuticals and an Alternative of Removal by Low-Cost Adsorbents: A Review. *Chemosphere* **2019**, *222*, 766−780.

(14) Li, M.; Gan, F.; Dong, J.; Fang, Y.; Zhao, X.; Zhang, Q. Facile Preparation of Continuous and Porous Polyimide Aerogel Fibers for Multifunctional Applications. *ACS Appl. Mater. Interfaces* **2021**, *13* (8), 10416−10427.

(15) Smyatskaya, Y.; Kosheleva, A.; Taranovskaya, E. Sorption Properties of Materials Based on Residual Biomass. *MATEC Web of Conferences*. EDP Sciences 2018 *245* 18005 .

(16) Ocampo-Perez, R.; Padilla-Ortega, E.; Medellin-Castillo, N. A.; Coronado-Oyarvide, P.; Aguilar-Madera, C. G.; Segovia-Sandoval, S. J.; Flores-Ramírez, R.; Parra-Marfil, A. Synthesis of Biochar from Chili Seeds and Its Application to Remove Ibuprofen from Water. Equilibrium and 3D Modeling. *Sci. Total Environ.* **2019**, *655*, 1397−1408.
(17) Hiyane, H.; Benkaddour, S.; Slimani, R.; Cagnon, B.; Karrouchi, K.; Haddad, M. E.; Achour, Y.; Antri, S. E.; Lazar, S. A Comparative Study Of Linear And Non-Linear Methods of Isotherm Parameters For Biosorption Of Sodium Diclofenac Onto Calcined Cow Leather (CCL). *Res. Sq.* **2021**. .
(18) da Costa, M. L.; Pavoski, G.; Espinosa, D. C. R.; de Vasconcellos, N. J. S.; da Silva, W. L. Potential Application of Alternative Materials for Organic Pollutant Removal. *Water, Air, Soil Pollut.* **2022**, *233* (2), 65−77.
(19) Souza, M. A. D.; Vilas-Boas, I. T.; Leite-da-Silva, J. M.; Abrahão, P. D. N.; Teixeira-Costa, B. E.; Veiga-Junior, V. F. Polysaccharides in Agro-Industrial Biomass Residues. *Polysaccharides* **2022**, *3* (1), 95−120.
(20) Cherubin, M. R.; Oliveira, D. M. D. S.; Feigl, B. J.; Pimentel, L. G.; Lisboa, I. P.; Gmach, M. R.; Varanda, L. L.; Morais, M. C.; Satiro, L. S.; Popin, G. V.; Paiva, S. R. D.; Santos, A. K. B. D.; Vasconcelos, A. L. S. D.; Melo, P. L. A. D.; Cerri, C. E. P.; Cerri, C. C. Crop Residue Harvest for Bioenergy Production and Its Implications on Soil Functioning and Plant Growth: A Review. *Sci. Agric.* **2018**, *75* (3), 255−272.
(21) Kumla, J.; Suwannarach, N.; Sujarit, K.; Penkhrue, W.; Kakumyan, P.; Jatuwong, K.; Vadthanarat, S.; Lumyong, S. Cultivation of Mushrooms and Their Lignocellulolytic Enzyme Production Through the Utilization of Agro-Industrial Waste. *Molecules* **2020**, *25* (12), 2811−2852.
(22) Freitas, L. C.; Barbosa, J. R.; da Costa, A. L. C.; Bezerra, F. W. F.; Pinto, R. H. H.; Carvalho Junior, R. N. D. From Waste to Sustainable Industry: How Can Agro-Industrial Wastes Help in the Development of New Products? *Resour., Conserv. Recycl.* **2021**, *169*, 105466−105480.
(23) Tsai, W.-T.; Jiang, T.-J.; Lin, Y.-Q.; Chang, H.-L.; Tsai, C.-H. Preparation of Porous Biochar from Soapberry Pericarp at Severe Carbonization Conditions. *Fermentation* **2021**, *7* (4), 228−237.
(24) Ferreira, A. F.; Ribau, J. P.; Costa, M. A Decision Support Method for Biochars Characterization from Carbonization of Grape Pomace. *Biomass Bioenergy* **2021**, *145*, 105946−105958.
(25) Qin, F.; Zhang, C.; Zeng, G.; Huang, D.; Tan, X.; Duan, A. Lignocellulosic Biomass Carbonization for Biochar Production and Characterization of Biochar Reactivity. *Renewable Sustainable Energy Rev.* **2022**, *157*, 112056−112082.
(26) Hassan, M. F.; Sabri, M. A.; Fazal, H.; Hafeez, A.; Shezad, N.; Hussain, M. Recent Trends in Activated Carbon Fibers Production from Various Precursors and Applications—A Comparative Review. *J. Anal. Appl. Pyrolysis* **2020**, *145*, 104715−104737.
(27) Wortmann, M.; Frese, N.; Mamun, A.; Trabelsi, M.; Keil, W.; Büker, B.; Javed, A.; Tiemann, M.; Moritzer, E.; Ehrmann, A.; Hütten, A.; Schmidt, C.; Gölzhäuser, A.; Hüsgen, B.; Sabantina, L. Chemical and Morphological Transition of Poly(Acrylonitrile)/Poly(Vinylidene Fluoride) Blend Nanofibers during Oxidative Stabilization and Incipient Carbonization. *Nanomaterials* **2020**, *10* (6), 1210−1231.
(28) Azman, A.; Ngadi, N.; Awg Zaini, D. K.; Jusoh, M.; Mohamad, Z.; Arsad, A. Effect of Adsorption Parameter on the Removal of Aspirin Using Tyre Waste Adsorbent. *Chem. Eng. Trans.* **2019**, *72*, 157−162.
(29) Oginni, O.; Singh, K.; Oporto, G.; Dawson-Andoh, B.; McDonald, L.; Sabolsky, E. Effect of One-Step and Two-Step H3PO4 Activation on Activated Carbon Characteristics. *Bioresour. Technol. Rep.* **2019**, *8*, 100307−100316.
(30) Karod, M.; Pollard, Z. A.; Ahmad, M. T.; Dou, G.; Gao, L.; Goldfarb, J. L. Impact of Bentonite Clay on In Situ Pyrolysis vs. Hydrothermal Carbonization of Avocado Pit Biomass. *Catalysts* **2022**, *12* (6), 655−669.
(31) Brito, M. J. P.; Veloso, C. M.; Santos, L. S.; Bonomo, R. C. F.; Fontan, R. D. C. I. Adsorption of the Textile Dye Dianix® Royal Blue CC onto Carbons Obtained from Yellow Mombin Fruit Stones and Activated with KOH and H3PO4: Kinetics, Adsorption Equilibrium and Thermodynamic Studies. *Powder Technol.* **2018**, *339*, 334−343.
(32) Cui, J.; Xu, X.; Yang, L.; Chen, C.; Qian, J.; Chen, X.; Sun, D. Soft Foam-like UiO-66/Polydopamine/Bacterial Cellulose Composite for the Removal of Aspirin and Tetracycline Hydrochloride. *Chem. Eng. J.* **2020**, *395*, 125174−125208.
(33) Rosset, M.; Sfreddo, L. W.; Perez-Lopez, O. W.; Féris, L. A. Effect of Concentration in the Equilibrium and Kinetics of Adsorption of Acetylsalicylic Acid on ZnAl Layered Double Hydroxide. *J. Environ. Chem. Eng.* **2020**, *8* (4), 103991−104000.
(34) Borges, R. F. O.; De Souza, R. S. V. A.; Vargas, M. L. V.; Scheid, C. M.; Calçada, L. A.; Meleiro, L. A. C. Analysis of the Stability of Oil-Based Drilling Muds by Electrical Stability Measurements as a Function of Oil-Water Ratio, Weighting Material and Lubricant Concentrations. *J. Pet. Sci. Eng.* **2022**, *218*, 110924−110941.
(35) Langmuir, I. The Dissociation of Hydrogen into Atoms. III. The Mechanism of the Reaction. *J. Am. Chem. Soc.* **1916**, *38*, 1145−1156.
(36) Nandwani, S. K.; Chakraborty, M.; Gupta, S. Adsorption of Surface Active Ionic Liquids on Different Rock Types under High Salinity Conditions. *Sci. Rep.* **2019**, *9* (1), 1−17.
(37) Enyoh, C. E.; Wang, Q.; Ovuoraye, P. E. Response Surface Methodology for Modeling the Adsorptive Uptake of Phenol from Aqueous Solution Using Adsorbent Polyethylene Terephthalate Microplastics. *Chem. Eng. J. Adv.* **2022**, *12*, 100370−100384.
(38) Suresh Kumar, P.; Korving, L.; Keesman, K. J.; van Loosdrecht, M. C. M.; Witkamp, G.-J. Effect of Pore Size Distribution and Particle Size of Porous Metal Oxides on Phosphate Adsorption Capacity and Kinetics. *Chem. Eng. J.* **2019**, *358*, 160−169.
(39) Freundlich, H. Über die Adsorption in Lösungen. *Z. Für Phys. Chem.* **1907**, *57* (1), 385−470.
(40) Batool, F.; Akbar, J.; Iqbal, S.; Noreen, S.; Bukhari, S. N. A. Study of Isothermal, Kinetic, and Thermodynamic Parameters for Adsorption of Cadmium: An Overview of Linear and Nonlinear Approach and Error Analysis. *Bioinorg. Chem. Appl.* **2018**, *2018*, 1−11.
(41) Chen, T.; Da, T.; Ma, Y. Reasonable Calculation of the Thermodynamic Parameters from Adsorption Equilibrium Constant. *J. Mol. Liq.* **2021**, *322*, 114980−114990.
(42) Sips, R. On the Structure of a Catalyst Surface. *J. Chem. Phys.* **1948**, *16* (5), 490−495.
(43) Vilardi, G.; Di Palma, L.; Verdone, N. Heavy Metals Adsorption by Banana Peels Micro-Powder: Equilibrium Modeling by Non-Linear Models. *Chin. J. Chem. Eng.* **2018**, *26* (3), 455−464.
(44) Benzaoui, T.; Selatnia, A.; Djabali, D. Adsorption of Copper (II) Ions from Aqueous Solution Using Bottom Ash of Expired Drugs Incineration. *Adsorpt. Sci. Technol.* **2018**, *36* (1−2), 114−129.
(45) Podder, M. S.; Majumder, C. B. Studies on the Removal of As(III) and As(V) through Their Adsorption onto Granular Activated Carbon/MnFe2O4 Composite: Isotherm Studies and Error Analysis. *Compos. Interfaces* **2016**, *23* (4), 327−372.
(46) Wakkel, M.; Khiari, B.; Zagrouba, F. Textile Wastewater Treatment by Agro-Industrial Waste: Equilibrium Modelling, Thermodynamics and Mass Transfer Mechanisms of Cationic Dyes Adsorption onto Low-Cost Lignocellulosic Adsorbent. *J. Taiwan Inst. Chem. Eng.* **2019**, *96*, 439−452.
(47) Munagapati, V. S.; Wen, J.-C.; Pan, C.-L.; Gutha, Y.; Wen, J.-H.; Reddy, G. M. Adsorptive Removal of Anionic Dye (Reactive Black 5) from Aqueous Solution Using Chemically Modified Banana Peel Powder: Kinetic, Isotherm, Thermodynamic, and Reusability Studies. *Int. J. Phytorem.* **2020**, *22* (3), 267−278.
(48) Yuh-Shan, H. Citation Review of Lagergren Kinetic Rate Equation on Adsorption Reactions. *Scientometrics* **2004**, *59* (1), 171−177.

https://doi.org/10.1021/acsomega.5c08131
ACS Omega 2025, 10, 57532−57544

(49) Alharby, N. F.; Almutairi, R. S.; Mohamed, N. A. Adsorption Behavior of Methylene Blue Dye by Novel CrossLinked O-CM-Chitosan Hydrogel in Aqueous Solution: Kinetics, Isotherm and Thermodynamics. *Polymers* **2021**, *13* (21), 3659−3687.
(50) Ho, Y. S.; McKay, G. A Kinetic Study of Dye Sorption by Biosorbent Waste Product Pith. *Resour., Conserv. Recycl.* **1999**, *25* (4), 171−193.
(51) Pholosi, A.; Naidoo, E. B.; Ofomaja, A. E. Intraparticle Diffusion of Cr(VI) through Biomass and Magnetite Coated Biomass: A Comparative Kinetic and Diffusion Study. *S. Afr. J. Chem. Eng.* **2020**, *32*, 39−55.
(52) Alaguprathana, M.; Poonkothai, M.; Ameen, F.; Ahmad Bhat, S.; Mythili, R.; Sudhakar, C. Sodium Hydroxide Pre-Treated Aspergillus Flavus Biomass for the Removal of Reactive Black 5 and Its Toxicity Evaluation. *Environ. Res.* **2022**, *214*, 113859−113869.
(53) Ali, A.; Javed, K.; Zahoor, I.; Anjum, K. M. Determination of the Best Non-Linear Function to Describe the Growth of Kajli Sheep. *S. Afr. J. Anim. Sci.* **2020**, *50* (3), 452−459.
(54) Calasan, M.; Abdel Aleem, S. H. E.; Zobaa, A. F. On the Root Mean Square Error (RMSE) Calculation for Parameter Estimation of Photovoltaic Models: A Novel Exact Analytical Solution Based on Lambert W Function. *Energy Convers. Manage.* **2020**, *210*, 112716−112732.
(55) Selvida, D.; Zarlis, M.; Situmorang, Z. Analysis of the Effect Early Cluster Centre Points on the Combination of K-Means Algorithms and Sum of Squared Error on k Centroid. *IOP Conf. Ser. : Mater. Sci. Eng.* **2020**, *725* (1), 012089−012096.
(56) Morley, S. K.; Brito, T. V.; Welling, D. T. Measures of Model Performance Based On the Log Accuracy Ratio. *Space Weather* **2018**, *16* (1), 69−88.
(57) Singh, S.; Mohanlall, V. Biocatalytic and Biological Activities of Cassia Occidentalis Mediated Silver Nanoparticles. *Trends Sci.* **2021**, *19* (1), 1712−1725.
(58) Htu, H. H.; San, H. H.; Swe, Z. M. Effects of Salinity on the Hatching Efficiency of Artemia Cysts Decapsulation. *Int. J. Sci. Eng. Appl.* **2019**, *8* (8), 341−344.
(59) Stalin, K.; Ravi, L.; Raghavan, V. Extraction Purification and Structural Elucidation of Environmentally Benign Antifouling Metabolite from Streptomyces Thermolineatus VITKV6A. *Environ. Technol. Innovation* **2022**, *25*, 102096−102105.
(60) Kisworo, D.; Sukirno; Bulkaini. Lethality Test of Some Varieties of Sea Cucumber Extract Against Artemia Salina, as Natural Food Additive in Meat-Based Functional Food. *Asian J. Appl. Res. Community Dev. Empowerment* **2021**, *5* (3), 7−10.
(61) Saravanan, N.; Sampath, P. S.; Sukantha, T. A. Extraction and Characterization of New Cellulose Fiber from the Agrowaste of Lagenaria Siceraria (Bottle Guard) Plant. *J. Adv. Chem.* **2016**, *12* (9), 4382−4388.
(62) Kusmono, K.; Affan, N. Isolation and Characterization of Nanocrystalline Cellulose from Ramie Fibers via Phosphoric Acid Hydrolysis. *J. Nat. Fibers* **2020**, *19*, 2744−2755.
(63) Asemani, M.; Rabbani, A. R. Detailed FTIR Spectroscopy Characterization of Crude Oil Extracted Asphaltenes: Curve Resolve of Overlapping Bands. *J. Pet. Sci. Eng.* **2020**, *185*, 106618−106631.
(64) Kostryukov, S. G.; Kalyazin, V. A.; Petrov, P. S.; Bezrukova, E. V.; Somov, N. V. 5-Arylpyrrolidine-2-Carboxylic Acid Derivatives as Precursors in the Synthesis of Sulphonyl-Substituted Pyrroles. *Russ. J. Org. Chem.* **2024**, *60* (2), 281−293.
(65) Çakmak, R.; Başaran, E.; Sahin, K.; Şentürk, M.; Durdağı, S. Synthesis of Novel Hydrazide−Hydrazone Compounds and *In Vitro* and *In Silico* Investigation of Their Biological Activities against AChE, BChE, and hCA I and II. *ACS Omega* **2024**, *9* (18), 20030−20041.
(66) De Freitas, A. G.; De Magalhães, B. E.; Minho, L. A.; Leão, D. J.; Santos, L. S.; Augusto De Albuquerque Fernandes, S. FTIR Spectroscopy with Chemometrics for Determination of Tylosin Residues in Milk. *J. Sci. Food Agric.* **2021**, *101* (5), 1854−1860.
(67) Zhou, J.; Liu, G.; Wang, S.; Zhang, H.; Xu, F. TG-FTIR and Py-GC/MS Study of the Pyrolysis Mechanism and Composition of Volatiles from Flash Pyrolysis of PVC. *J. Energy Inst.* **2020**, *93* (6), 2362−2370.
(68) Jiao, A.; Tian, S.; Lin, H. Analysis of Outburst Coal Structure Characteristics in Sanjia Coal Mine Based on FTIR and XRD. *Energies* **2022**, *15* (6), 1956−1970.
(69) Yao, W.; Weng, Y.; Catchmark, J. M. Improved Cellulose X-Ray Diffraction Analysis Using Fourier Series Modeling. *Cellulose* **2020**, *27* (10), 5563−5579.
(70) Thommes, M.; Kaneko, K.; Neimark, A. V.; Olivier, J. P.; Rodriguez-Reinoso, F.; Rouquerol, J.; Sing, K. S. W. Physisorption of Gases, with Special Reference to the Evaluation of Surface Area and Pore Size Distribution (IUPAC Technical Report). *Pure Appl. Chem.* **2015**, *87* (9−10), 1051−1069.
(71) Song, X.; Zhou, X.; Lv, X. Quantitative Evaluation of Pore Connectivity of Shales with a Type H3 Sorption Hysteresis Loop. *J. Asian Earth Sci.* **2023**, *247*, 105595−105609.
(72) Ramasamy, L.; Miranda, L. R. Surface-Modified Adsorbent from Artocarpus Heterophyllus Lam Biomass to Confine Reactive Red 194 in Real and Synthetic Effluents: Kinetics and Equilibrium Study. *Adsorpt. Sci. Technol.* **2022**, *2022*, 1−23.
(73) Nguyen, P. X. T.; Ho, K. H.; Do, N. H. N.; Nguyen, C. T. X.; Nguyen, H. M.; Tran, K. A.; Le, K. A.; Le, P. K. A Comparative Study on Modification of Aerogel-Based Biosorbents from Coconut Fibers for Treatment of Dye- and Oil-Contaminated Water. *Mater. Today. Sustainability* **2022**, *19*, 100175−100188.
(74) Bari, M. N.; Muna, F. Y.; Rahnuma, M.; Hossain, M. I. Production of Activated Carbon From Rice Husk and Its Proximate Analysis. *J. Eng. Sci.* **2022**, *13* (1), 105−112.
(75) Dhawane, S. H.; Kumar, T.; Halder, G. Recent Advancement and Prospective of Heterogeneous Carbonaceous Catalysts in Chemical and Enzymatic Transformation of Biodiesel. *Energy Convers. Manage.* **2018**, *167*, 176−202.
(76) Trinh, B.-S.; Le, P. T. K.; Werner, D.; Phuong, N. H.; Luu, T. L. Rice Husk Biochars Modified with Magnetized Iron Oxides and Nano Zero Valent Iron for Decolorization of Dyeing Wastewater. *Processes* **2019**, *7* (10), 660−677.
(77) Dou, S.; Ke, X.-X.; Shao, Z.-D.; Zhong, L.-B.; Zhao, Q.-B.; Zheng, Y.-M. Fish Scale-Based Biochar with Defined Pore Size and Ultrahigh Specific Surface Area for Highly Efficient Adsorption of Ciprofloxacin. *Chemosphere* **2022**, *287*, 131962−131971.
(78) Tomul, F.; Arslan, Y.; Kabak, B.; Trak, D.; Tran, H. N. Adsorption Process of Naproxen onto Peanut Shell-derived Biosorbent: Important Role of $n - \pi$ Interaction and van Der Waals Force. *J. Chem. Technol. Biotechnol.* **2021**, *96* (4), 869−880.
(79) Abiodun, O.-A. O.; Oluwaseun, O.; Oladayo, O. K.; Abayomi, O.; George, A. A.; Opatola, E.; Orah, R. F.; Isukuru, E. J.; Ede, I. C.; Oluwayomi, O. T.; Okolie, J. A.; Omotayo, I. A. Remediation of Heavy Metals Using Biomass-Based Adsorbents: Adsorption Kinetics and Isotherm Models. *Clean Technol.* **2023**, *5* (3), 934−960.
(80) Conde-González, J. E.; Lorenzo-Luis, P.; Salvadó, V.; Havel, J.; Peña-Méndez, E. M. A New Cotton Functionalized with Iron(III) Trimer-like Metal Framework as an Effective Strategy for the Adsorption of Triarylmethane Dye: An Insight into the Dye Adsorption Processes. *Heliyon* **2021**, *7* (12), No. e08524.
(81) Bullen, J. C.; Saleesongsom, S.; Gallagher, K.; Weiss, D. J. A Revised Pseudo-Second-Order Kinetic Model for Adsorption, Sensitive to Changes in Adsorbate and Adsorbent Concentrations. *Langmuir* **2021**, *37* (10), 3189−3201.
(82) Saadi, R.; Saadi, Z.; Fazaeli, R.; Fard, N. E. Monolayer and Multilayer Adsorption Isotherm Models for Sorption from Aqueous Media. *Korean J. Chem. Eng.* **2015**, *32* (5), 787−799.
(83) Abdel-Rahman, F. A.; Khafagi, E. Y.; Soliman, M. S.; Shoala, T.; Ahmed, Y. Preharvest Application of Salicylic Acid Induces Some Resistant Genes of Sweet Pepper against Black Mold Disease. *Eur. J. Plant Pathol.* **2021**, *159* (4), 755−768.
(84) Cheng, Y.; Wang, B.; Shen, J.; Yan, P.; Kang, J.; Wang, W.; Bi, L.; Zhu, X.; Li, Y.; Wang, S.; Shen, L.; Chen, Z. Preparation of Novel N-Doped Biochar and Its High Adsorption Capacity for Atrazine

https://doi.org/10.1021/acsomega.5c08131
ACS Omega 2025, 10, 57532−57544

Based on $\pi-\pi$ Electron Donor-Acceptor Interaction. *J. Hazard. Mater.* **2022**, *432*, 128757.
(85) Ban, S.-E.; Lee, E.-J.; Lim, D.-J.; Kim, I.-S.; Lee, J.-W. Evaluation of Sulfuric Acid-Pretreated Biomass-Derived Biochar Characteristics and Its Diazinon Adsorption Mechanism. *Bioresour. Technol.* **2022**, *348*, 126828.
(86) Jabar, J. M.; Adebayo, M. A.; Odusote, Y. A.; Yılmaz, M.; Rangabhashiyam, S. Valorization of Microwave-Assisted H3PO4-Activated Plantain (Musa Paradisiacal L) Leaf Biochar for Malachite Green Sequestration: Models and Mechanism of Adsorption. *Results Eng.* **2023**, *18*, 101129−101138.
(87) Wang, J.; Tan, Y.; Yang, H.; Zhan, L.; Sun, G.; Luo, L. On the Adsorption Characteristics and Mechanism of Methylene Blue by Ball Mill Modified Biochar. *Sci. Rep.* **2023**, *13* (1), 21174−21185.
(88) Varela, C. F.; Moreno-Aldana, L. C.; Agámez-Pertuz, Y. Y. Adsorption of Pharmaceutical Pollutants on $ZnCl_2$-Activated Biochar from Corn Cob: Efficiency, Selectivity and Mechanism. *J. Bioresour. Bioprod.* **2024**, *9* (1), 58−73.
(89) Bang, S. H.; Hong, N.-H.; Ahn, J.-Y.; Sekhon, S. S.; Kim, Y.-H.; Min, J. Proteomic Analysis of Daphnia Magna Exposed to Caffeine, Ibuprofen, Aspirin and Tetracycline. *Toxicol. Environ. Health Sci.* **2015**, *7* (2), 97−104.
(90) Caldas, L. L.; Moreira, R. A.; Espíndola, E. L. G.; Novelli, A. Environmental Risk Assessment of Drugs in Tropical Freshwaters Using Ceriodaphnia Silvestrii as Test Organism. *Bull. Environ. Contam. Toxicol.* **2023**, *110* (6), 106−113.
(91) Cleuvers, M. Mixture Toxicity of the Anti-Inflammatory Drugs Diclofenac, Ibuprofen, Naproxen, and Acetylsalicylic Acid. *Ecotoxicol. Environ. Saf.* **2004**, *59* (3), 309−315.
(92) Cuiping, H.; Na, Z.; Limei, H.; Tang, T.; Yang, Y.; Xiangping, N. Assessment of Ecotoxicity Effects of Aspirin on Non-Target Organism (*Daphnia Magna*) via Analysis of the Responses of Oxidative Stress, DNA Methylation-Related Genes Expressions and Life Traits Changes. *Ecotoxicology* **2023**, *32* (2), 137−149.
(93) Da Silva, A. Q.; De Souza Abessa, D. M. Toxicity of Three Emerging Contaminants to Non-Target Marine Organisms. *Environ. Sci. Pollut. Res.* **2019**, *26* (18), 18354−18364.

https://doi.org/10.1021/acsomega.5c08131
ACS Omega 2025, 10, 57532−57544